

AN ADVANCED THREE PHASE FOUR WIRE GRID TIED WIND ENERGY SYSTEM USING SVPWM CONTROL

¹A SHRAVAN KUMAR, ²K VAMSEE KRISHNA

¹M Tech, Vignana Bharathi Institute of Technology, Hyderabad

²Associate Professor, Vignana Bharathi Institute of Technology, Hyderabad

ABSTRACT- This paper proposes a control structure in three phase four wire system that provides more functionality to the grid side converter of a wind turbine system using the CPT as an alternative for generating different current references for selective disturbances compensation, where both single and three phase loads are fed. Three phase, four wire inverters proposed using conventional three leg converters with “split capacitor” (OR) four leg converters. In a three leg conventional converter, the AC neutral wire is directly connected to the electrical midpoint of the DC bus. In this system consist of single and three phase linear and nonlinear (balanced and unbalanced) loads. The CPT is used to identify and to quantify the amount of resistive, reactive unbalanced and nonlinear characteristics of a particular load under different supply voltage conditions for four wire system. The control structure was tested with a comprehensive real time benchmarking case study with hardware in the loop. The control algorithms were compiled inside on DSP and validated using the real time system “OPAL-RT”. As an extension replacing the existing control technique with the advanced SVPWM (space vector pulse width modulation) control strategy. By using this technique complexity of the system will be decreased, disturbances are reduced and power quality is improved. Therefore efficiency of the system is improved.

Index Terms—Conservative Power Theory (CPT), Four-Leg Voltage Source Converter (VSC), Hardware-In-The-Loop (HIL), Permanent Magnet Synchronous Generator (PMSG), Power Quality, SVPWM Techniques.

1. INTRODUCTION

In recent years, wind energy has become one of the most important and promising sources of renewable energy, which demands additional transmission capacity and better means of maintaining system reliability. To have sustainable growth and social progress, it is necessary to meet the energy need by utilizing the renewable energy resources like wind. The need to integrate the renewable energy like wind energy into power system is to make it possible to minimize the environmental impacts. Wind energy conversion systems are the fastest growing renewable source of electrical energy having tremendous environmental, social, and economic benefits.

Power Quality is defined as power that enables the equipment to work properly. A power quality problem can be defined as any deviation of magnitude, frequency, or purity from the ideal

sinusoidal voltage waveform. Good power quality is benefit to the operation of electrical equipment, but poor power quality will produce great harm to the power system. However, the generated power from wind energy conversion system is always fluctuating due to the fluctuation nature of the wind. Therefore injection of the wind power into an electric grid affects the power quality. The important factors to be considered in power quality measurement are the active power, reactive power, variation of voltage, flicker, harmonics, and electrical behavior of switching operation.

Several control approaches have been introduced in the literature for wind turbine in standalone and grid connected system. The grid side controllers are designed to ensure active and reactive power is delivered to the grid. In order to allow the theoretical framework, different power theories have been proposed and implemented in electrical power systems to analyze current and voltage components, such as the instantaneous power (PQ) theory for a three-phase system made by Akagi. In PQ theory, the three-phase is transformed into a two-phase reference frame in order to extract active and reactive components in a simplified manner. A three-phase power theory in a broader perspective has been introduced, known as the conservative power theory (CPT), where the current and voltage components are derived in the three-phase form, without requiring any reference-frame transformation. The performance of these theories has been compared. This paper proposes a control structure in three-phase four wire systems that provide more functionality to the grid-side converter of a wind turbine system using the CPT as an alternative to generating different current references for selective disturbances compensation, where both single- and three-phase loads are fed. Three-phase, four-wire inverters have been realized using conventional three-leg converters with “split capacitor” or four-leg converters.

In a three-leg conventional converter, the ac neutral wire is directly connected to the electrical midpoint of the dc bus. In four-leg converter, the ac neutral wire connection is provided through the fourth switch leg. The “four-leg” converter topology has better controllability than the “split-capacitor” converter topology. The considered system consists of single- and three-phase linear and nonlinear

(balanced and unbalanced) loads. The CPT is used to identify and to quantify the amount of resistive, reactive, unbalanced, and nonlinear characteristics of a particular load under different supply voltages condition for four-wire system.

The organization of the paper is as follows. Section II presents the utility-connected wind turbine system considered in this paper. In Section III, a brief review of the CPT for three-phase circuits is presented. Section IV presents the control design of the back-to-back converter system. Section V is dedicated to the experimental verification of the proposed control structure through a real-time hardware-in-the-loop (HIL) setup. Finally, the conclusion of this paper is presented in Section VI.

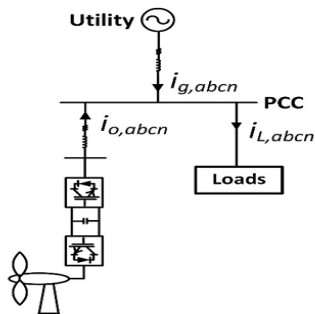


Fig.1. Single line diagram of the addressed industrial system with wind turbine system

2. SYSTEM CONFIGURATION

Fig.1 shows a diagram of a utility connected industrial system addressed in this paper. The structure of the power converter used in the wind turbine system is a back-to-back converter with a permanent magnet synchronous generator (PMSG) connected to the same bus with the loads. The loads are a combination of linear and highly inductive loads causing harmonics at the point of common coupling (PCC).

3. CONSERVATIVE POWER THEORY

The CPT decomposes the power and current in the stationary frame, according to terms directly related to electrical characteristics, such as average power transfer, reactive energy, unbalanced loads and nonlinearities. Assuming a generic poly-phase circuit under periodic operation (period T), where (v) and (i) are, respectively, the voltage and current vectors, and (∫ v) is the unbiased integral of the voltage vector measured at a given network port (phase variables are indicated with subscript “m”), the CPT authors define.

1) Instantaneous active power
$$P(t) = \underline{v} \cdot \underline{i} = \sum_{m=1}^M v_m i_m \tag{1}$$

2) Instantaneous reactive energy
$$w(t) = \underline{\hat{v}} \cdot \underline{i} = \sum_{m=1}^M \hat{v}_m i_m \tag{2}$$

The corresponding average values of (1) and (2) are the active power and reactive energy defined in (3) and (4), respectively as follows:

$$P = \bar{P} = \underline{v} \cdot \underline{\hat{i}} = \frac{1}{T} \int_0^T \underline{v} \cdot \underline{\hat{i}} dt = \sum_{m=1}^M P_m \tag{3}$$

$$W = \bar{W} = \underline{\hat{v}} \cdot \underline{i} = \frac{1}{T} \int_0^T \underline{\hat{v}} \cdot \underline{i} dt = \sum_{m=1}^M W_m \tag{4}$$

The phase currents are decomposed into three current components as follows. Active phase currents are defined by

$$\underline{i}_{am} = \frac{v_m \cdot i_m}{\|v_m\|} v_m = \frac{P_m}{v_m^2} v_m = G_m v_m \tag{5}$$

Where (G_m) is the equivalent phase conductance. Reactive phase currents are given by

$$\underline{i}_{rm} = \frac{\hat{v}_m i_m}{\|\hat{v}_m\|} \hat{v}_m = \frac{W_m}{\hat{v}_m^2} \hat{v}_m = B_m \hat{v}_m \tag{6}$$

Where (B_m) is the equivalent phase reactivity. Void phase currents are the remaining current terms

$$\underline{i}_{vm} = \underline{i}_m - \underline{i}_{am} - \underline{i}_{rm} \tag{7}$$

Where they convey neither active power nor reactive energy. The active and reactive phase currents can be further decomposed into balanced and unbalanced terms. The balanced active currents have been defined as

$$\underline{i}_{am}^b = \frac{\underline{v} \cdot \underline{i}}{\|v\|^2} v_m = \frac{P}{v^2} v_m = G^b v_m \tag{8}$$

And such currents represent the minimum portion of the phase currents, which could be associated with a balanced equivalent circuit, responsible for conveying the total active power (P) in the circuit, under certain voltage conditions. The balanced reactive currents have been defined as

$$\underline{i}_{rm}^b = \frac{\underline{\hat{v}} \cdot \underline{i}}{\|\hat{v}\|^2} \hat{v}_m = B^b \hat{v}_m \tag{9}$$

And they represent the minimum portion of the phase currents, which could be associated with a balanced equivalent circuit, responsible for conveying the total reactive energy (W) in the circuit. The imbalanced active currents are calculated by difference between (5) and (8)

$$\underline{i}_{am}^u = \underline{i}_{am} - \underline{i}_{am}^b = (G_m - G^b) v_m \tag{10}$$

In the same way, the imbalanced reactive currents are

$$\underline{i}_{rm}^u = \underline{i}_{rm} - \underline{i}_{rm}^b = (B_m - B^b) \hat{v}_m \tag{11}$$

Thus, the total imbalance phase current vector is defined as

$$\underline{i}_m^u = \underline{i}_{am}^u + \underline{i}_{rm}^u \tag{12}$$

The current vector can be given as

$$\underline{i} = \underline{i}_a^b + \underline{i}_r^b + \underline{i}_a^u + \underline{i}_r^u + \underline{i}_v \tag{13}$$

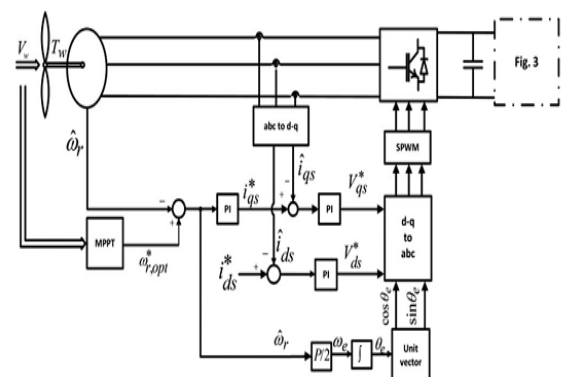


Fig.2. Control scheme of machine side converter

4. CONTROL DESIGN

A. Machine Side Controller

The purpose of the machine side converter is to track the optimum point of the rotor to extract the maximum power existing in the turbine. For a given wind turbine, the maximum power occurs at the maximum power coefficient of the turbine. For a given wind speed, there is an optimum rotor speed that gives the optimum tip speed ratio

$$\lambda_{opt} = \frac{R_w \omega_{w,opt}}{v_w} \tag{14}$$

By knowing the tip speed ratio of the wind turbine, one can extract the maximum power from the rotor by calculating the optimum rotor speed as

$$\omega_{w,opt} = \frac{v_w \lambda_{opt}}{R_w} \tag{15}$$

Then, this optimum rotor reference is subtracted from the measured rotor speed to produce the speed error. As shown in Fig. 2, a rotor speed controller is designed to generate the quadrature current reference to the internal current controller. The direct current reference in this paper is set to zero. The detail of the controller design procedure is presented. The parameters and values of the grid-side system and the load are illustrated in Table I.

B. Grid-Side Controller

In this section, the current-controlled voltage source inverter is designed and modeled. The control scheme for the four-leg grid-side inverter is shown in Fig. 3. Fig. 3 illustrates the schematic diagram of the grid-tied four leg inverter unit, consisting of a four-leg voltage source converter (VSC) and the network

load that are connected to the distribution network at PCC. The inductance of the filter is L_f and R_f is the ohmic loss of the inductor. The machine side converter of Fig. 2 is connected in parallel with the VSC de-link capacitor C_{dc} . It is shown that the grid-side inverter unit is controlled in an abc-reference frame. v_{pcc} is dictated by the grid representing the PCC/load voltage. The control objective is to allow the wind source to inject its available energy, as well as to work as an active power filter for improving power quality based on CPT functionalities. Fig. 4 shows the circuit, containing both balanced and unbalanced linear and nonlinear loads. The parameters and values of the grid-side system and the load are illustrated in Table II.

TABLE I
PMSG PARAMETERS
AND WIND TURBINE SPECIFICATIONS

Parameters	Values
Stator resistance, R_s	0.672 Ω
d-axis leakage inductance, L_d	13.74 mH
q-axis leakage inductance, L_q	13.74 mH
Flux linkage, ψ_m	2.39 Wb
Number of poles of machines, P	24
Voltage	500 V
Nominal output power of wind turbine	10 kW
Base wind speed	10 m/s
Base rotor speed	200 r/min

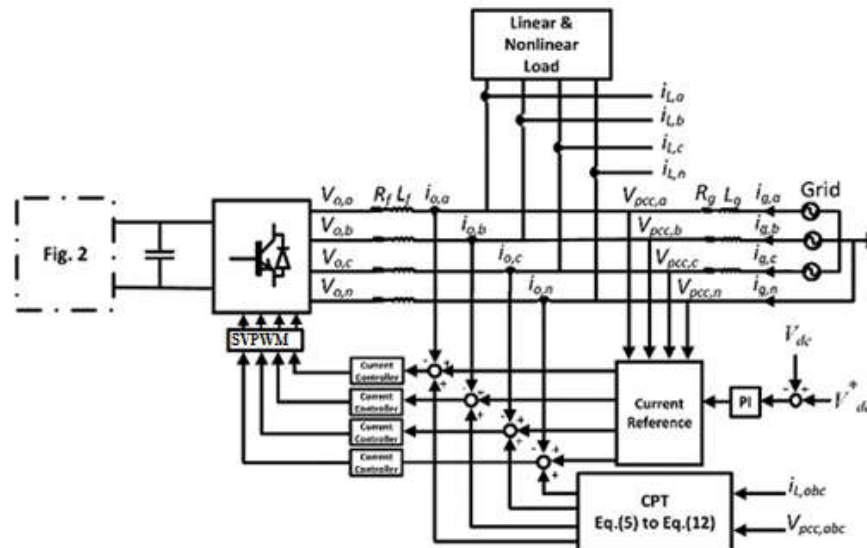


Fig.3. Control scheme of a grid-side converter

The inverter unit control system consists of two feedback control loops. The first loop demonstrated in Fig. 5 is a fast loop controlling the output current, showing that $i_{o,abcn}$ can rapidly track their respective reference commands $i^*_{o,abcn}$, while $i^*_{o,n}$ is determined as $i^*_{o,n} = -(i^*_{o,a} + i^*_{o,b} + i^*_{o,c})$. The outer loop depicted in Fig. 8 is a slower loop regulating the dc-link voltage. The dc-link keeps the power balance between the power which is delivered to the system in the output of the inverter and the power in the dc-link. The desired inverter output current is the summation of the active current provided from the wind (i_{active}) and the compensation of unwanted load current disturbances delivered by the CPT technique. The block diagram of the system in the “s” plane shown in Fig. 5 is designed in an abc frame based on the classical frequency response analysis method.

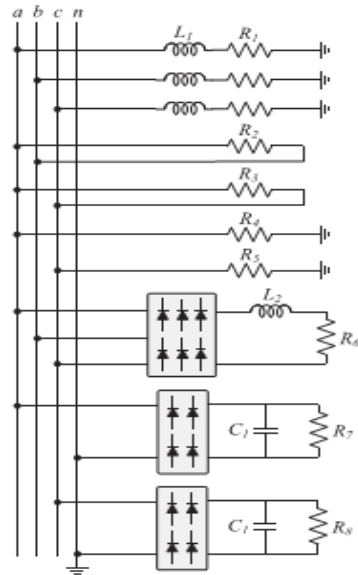


Fig. 4. Schematic diagram of the configurable load in Fig. 3

Consider the grid-tied four-leg inverter of Fig. 3 and the current control loop block diagram of Fig. 5; the dynamics of the ac-side currents $i_{o,abcn}(t)$ are described by (16) and (17). Equation (16) represents a system in which $i_{o,abcn}(t)$ are the state variables, $v_{o,abcn}(t)$ are the control inputs, and $v_{pcc,abcn}(t)$ are the disturbance inputs. Based on (17), the control input $v_{o,abcn}(t)$ are proportional to, and can be controlled by, the modulating signal $m_{o,abcn}(t)$. The transfer function of the current control scheme, $G_i(s)$, is determined as in (18). The first step to perform the controller design is to obtain the open-loop current transfer function $G_{oi}(s)$ as expressed in (19) with $C_i(s)$ the controller of the current control loop, consisting of a lag compensator as (20), where the parameters of

ω_z , ω_p , and k_c are the zero, pole, and the gain of the compensator, respectively. Furthermore, the voltage feed-forward compensation is employed to mitigate the dynamic couplings between the four-leg inverter and the ac system, enhancing the disturbance rejection capability of the converter system.

TABLE II
GRIDSIDESYSTEM ANDLOADPARAMETERS

Parameters	Values
Nominal grid pick phase voltage, v_{pcc}	180 V
Grid frequency, f	60 Hz
Switching frequency, f_s	12 kHz
Output filter inductor, L_f	10 mH
Output filter resistor, R_f	0.1 Ω
DC link voltage reference, V_{dc}	1000 V
DC-link capacitor, C_{dc}	5 mF
Grid inductor, L_g	3 mH
Grid resistor, R_g	1 Ω
Load inductor, L_1	30 mH
Load inductor, L_2	4 mH
Load capacitor, C_1	220 μ F
Load resistor, R_1	1 Ω
Load resistor, R_2	80 Ω
Load resistor, R_3	35 Ω
Load resistor, R_4	30 Ω
Load resistor, R_5	40 Ω
Load resistor, R_6	200 Ω
Load resistor, R_7	150 Ω
Load resistor, R_8	200 Ω

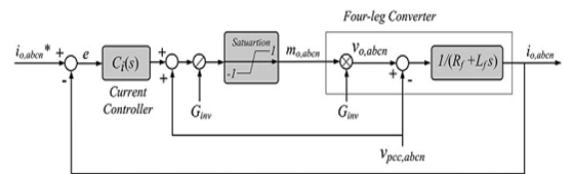


Fig.5. Block diagram of the current control loop

$$L_f \frac{di_{o,abcn}(t)}{dt} + R_f i_{o,abcn}(t) = v_{o,abcn}(t) - v_{pcc,abcn}(t) \quad (16)$$

$$v_{o,abcn}(t) = G_{inv} m_{o,abcn}(t) = \left(\frac{V_{dc}}{2}\right) m_{o,abcn}(t) \quad (17)$$

$$G_i(s) = \frac{i_{o,abcn}(s)}{v_{o,abcn}(s)} = \frac{1}{L_f s + R_f} \quad (18)$$

$$G_{oi}(s) = \frac{C_i(s)}{R_f + sL_f}, \quad (19)$$

$$C_i(s) = \frac{k_c \left(1 + \frac{s}{\omega_z}\right)}{\left(1 + \frac{s}{\omega_p}\right)} \quad (20)$$

The Plant transfer function in z-domain is obtained by means of the z-transformation. The z-transformation of a transfer function in s-domain,

combined to a zero-order holder, is given by (21). Transformation is made using the relation $z = e^{sT_s}$. So, $G_i(z)$ can be defined as follows:

$$G_i(z) = Z \left\{ \frac{(1 - e^{-sT_s}) G_i(s)}{s} \right\} \quad (21)$$

$$G_i(z) = (1 - Z^{-1}) Z \left\{ \frac{G_i(s)}{s} \right\} \quad (22)$$

To allow the use of the frequency response method design, the conversion of $G_i(z)$ transfer function from “z” plane to “w” plane is performed using the bilinear transform shown in (23)

$$z = \frac{1 + \frac{T_s}{2} w}{1 - \frac{T_s}{2} w} \quad (23)$$

From where comes

$$G_i(w) = \frac{-0.0041w + 100}{w + 10} \quad (24)$$

Fig. 6 presents a comparison between the frequency response of system transfer function $G_i(s)$, and digitalized plant $G_i(w)$. It is noticeable that the frequency response presents conformity.

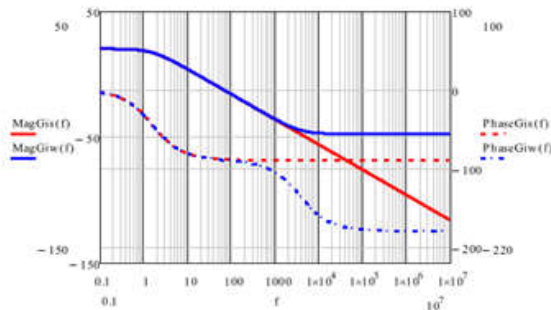


Fig.6. Gain and the phase of the current control plant in both “s”and“w” planes.

up to 3 kHz, when the phase error goes by substantial caused by the zero added because of the digitalization process. The crossover frequency of the current controller is chosen to be one-tenth of switching frequency. For $f_{ci} = 1.2$ kHz, $\phi_{PMi} = 72^\circ$, and $f_z = f_{ci}/10 = 120$ Hz, the rest of parameters in (20) are calculated as $f_p = 106.6$ Hz and $k_c = 80.88$. The frequency response of the open-loop transfer function is illustrated in Fig. 7.

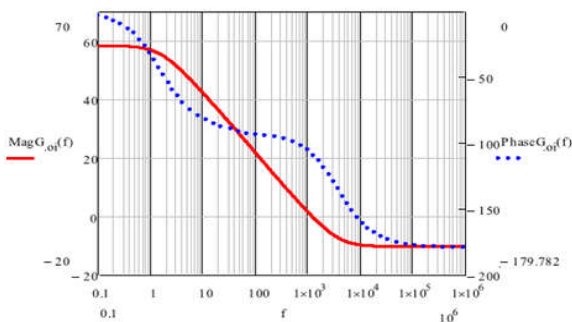


Fig. 7. Bode plot of the open-loop current transfer function.

The crossover frequency of the current controller is chosen to be one-tenth of switching frequency. For $f_{ci} = 1.2$ kHz, $\phi_{PMi} = 72^\circ$, and $f_z = f_{ci}/10 = 120$ Hz, the rest of parameters in (20) are calculated as $f_p = 106.6$ Hz and $k_c = 80.88$. The frequency response of the open-loop transfer function is illustrated in Fig. 7. It can be seen that at crossover frequency, the open loop gain of 0 dB and the phase margin of 72° are obtained.

The output current behavior of the grid-tied four-leg inverter can be described by (25). It can be seen that the output current only depends on the reference current. In other words, under the feed-forward compensation, the converter system is equivalent to an independent current source as viewed by the ac system

$$i_{0,abcn}(s) = \frac{C_i(s)}{L_f s + R_f + C_i(s)} i_{0,abcn}^*(s) \quad (25)$$

For digital implementation of the control system in the z-domain, the controller of (20) is discredited by the bilinear transform with a sampling time of T_s that is also the switching period [24]. Therefore, the controller transfer function $C_i(z)$

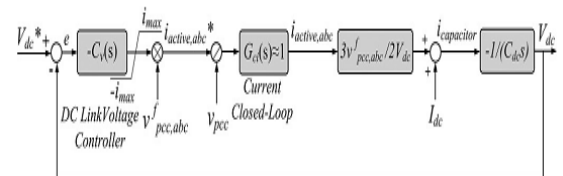


Fig.8. Block diagram of the dc voltage control loop can be expressed as (26)

$$C_i(z) = \frac{72.1z - 67.7}{z - 0.94} \quad (26)$$

The current reference, $i_{active,abc}$, is used to inject the active power delivered from the wind through the inverter. The waveform of the active current reference is defined from the fundamental component of the measured load voltage, $v_{pcc,abc}^f$, configuring sinusoidal current. Therefore, the active current is a pure sinusoidal current, in phase with the fundamental component of the instantaneous load voltage. Dimensioning of the dc-link voltage controller is determined by the transfer function between the defined current reference and the dc-link voltage. From power balance of the inverter terminal, we have

$$P_{ac} + P_{wind} + P_{cap} = 0 \quad (27)$$

$$\frac{3}{2} v_{pcc,abc}^f i_{active,abc} + V_{dc} I_{dc} + V_{dc} i_{capacitor} = 0 \quad (28)$$

Where $i_{capacitor}$ is the dc-link capacitor current and $3/2$ factor comes from the average ac power flow using peak values and $v_{pcc,abcn}^f$ represents the fundamental

component of the PCC voltage. From (28) the current through the capacitor is

$$i_{capacitor} = -\left(\frac{3V_{pcc,abc}^{f} i_{active,abc}}{2V_{dc}} + I_{dc}\right). \quad (29)$$

The same current in terms of voltage across the capacitor is given by

$$C_{dc} \frac{dV_{dc}}{dt} = i_{capacitor} \quad (30)$$

From (29) and (30), the differential equation for the dc-link voltage becomes

$$\frac{dV_{dc}}{dt} = -\frac{1}{C_{dc}} \left(\frac{3V_{pcc,abc}^{f} i_{active,abc}}{2V_{dc}} + I_{dc}\right). \quad (31)$$

Based on (31) the dc voltage is regulated by controlling the active current $i_{active,abc}$. The block diagram of the dc voltage control is shown in Fig. 8. The dc-link voltage controller $C_{vdc}(s)$ is multiplied by -1 to compensate for the negative sign of dc bus voltage dynamics. We will select the bandwidth of dc voltage loop to be less than two orders of magnitude smaller than that of the current loop. Therefore, the closed current loop can be assumed ideal for design purposes and replaced by unity. The transfer functions of dc-link voltage control scheme, $G_{vdc}(s)$, is presented in (32). The open-loop transfer functions of the dc voltage control loop, $G_{ovdc}(s)$, is presented in (33) with $C_v(s)$ the controller

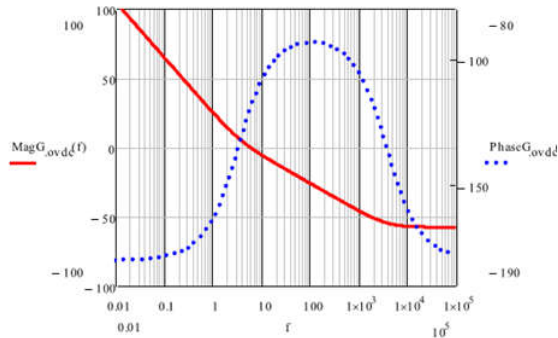


Fig. 9. Bode plot of the open loop dc-link voltage transfer function.

of the dc voltage control loop, consisting of a proportional integral compensator as in (34), where the parameters of k_p and k_i are the proportional and integral gains of the compensator, respectively,

$$G_{vdc}(s) = \frac{3V_{pcc,abc}^{f}}{2V_{dc}} \frac{1}{C_{dc} s} \quad (32)$$

$$G_{ovdc}(s) = C_v(s) G_{vdc}(s) \quad (33)$$

$$C_v(s) = \frac{k_p s + k_i}{s} \quad (34)$$

For DSP implementation of the dc-link voltage control scheme, $G_{vdc}(s)$ is converted from continuous plane “s” to the discrete plane “z” in (35). To allow the use of frequency response method design, the

conversion of $G_{vdc}(z)$ transfer function from “z” plane to “w” plane in (36) is performed, using the bilinear transform of (23)

$$G_{vdc}(z) = (1-z^{-1})Z\left\{\frac{G_{vdc}(s)}{s}\right\} \quad (35)$$

$$G_{vdc}(w) = \frac{-0.00225w+54}{w} \quad (36)$$

The crossover frequency of the dc voltage loop is chosen to be $f_{c_{vdc}}=6$ Hz and the phase margin $\phi_{PM_{vdc}}$ is selected to be 60° . We can compute that $k_p=0.6$ and $k_i=13.12$. Fig. 9 shows the frequency response of the open-loop dc-link voltage control scheme. It can be seen that at cross over frequency, the open loop gain of 0 dB and the phase margin of 60° are obtained. The dc-link voltage controller $C_v(s)$ is also discretized for digital implementation using the bilinear transform with a sampling time of T_s that is also the switching period. Therefore, the controller transfer function $C_v(z)$ can be expressed as follows:

$$C_v(z) = \frac{0.6z-0.6}{z-1} \quad (37)$$

5. REAL-TIME SIMULATION IN THE LOOP RESULTS

The proposed industrial system with the wind turbine shown in Fig. 1 was modeled and compiled using the well-known real-time simulator Opal-RT. Opal-RT allows precise benchmarking of real-time controllers, with specific sampling for specific control blocks. After an Opal-RT study such as this one, it is possible to generate C code for accurate compilation on real-time kernels or real-time operating systems, usually implemented with DSP hardware.

The specification of the wind turbine was selected in accordance to those parameters. The wind turbine has an optimum wind speed of 200 r/m IN at 10-m/s rated wind speed. The load parameters listed in Table II are used in the model.

The control algorithm was implemented using HIL. The wind turbine model with the grid connected back-to-back converter and power grid were built inside Matlab/Simulink. Then, the system was compiled inside the real-time simulator “Opal-RT.” The CPT theory was coded inside the DSP along with the current controllers. A sampling frequency of 12 kHz is used to discretize the signals. The test is implemented for various cases. The scaling for phase voltages, phase, and neutral currents per division are 60 V, 15A and 5 A, respectively.

A. Active Power Delivery

In this case study, the four-leg inverter is set to deliver active power produced by the wind to the load, ($i_{ref}=i_{active}$), and the remaining active power is delivered to the grid with unity power factor without doing any compensation strategy. Fig. 10(a) shows the inverter voltage is in phase with the inverter current meaning only active power is delivered to the

load and grid. From Fig. 10(b), the grid currents are unbalanced and distorted showing the requirement for power quality improvement. In Fig. 10(c), it is clear that the utility is supplying the linear and nonlinear single loads through its neutral wire while the inverter neutral current is zero.

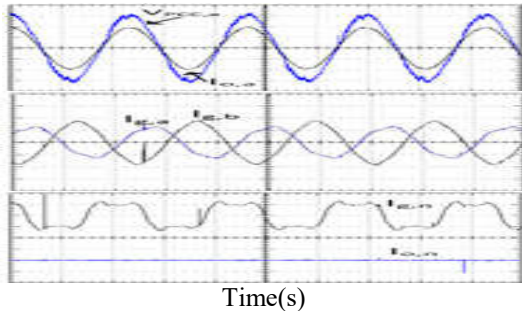


Fig.10. Active power delivery: (a) PCC voltage and inverter current; (b) two phases of grid currents; and (c) grid neutral current ($I_{g,n}$) and inverter neutral current ($I_{o,n}$).

B. Active and Reactive Power Delivery

In Fig. 11, the controller is set to supply the balance reactive current/power component of the load besides the delivery of active power ($i_{ref} = i_{active} + i_{br}$). From the voltage and current waveforms shown in Fig. 11(a), the inverter is supplying active and reactive power since the inverter current is no longer in phase with the voltage. The result of this compensation strategy is shown in Fig. 11(b) in which the void and unbalance current components of the load is supplied by the grid. It can be seen from Fig. 11(c) the grid is supplying the neutral current, related to single phase loads.

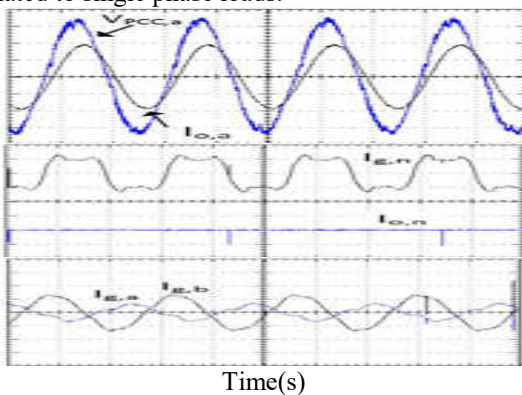


Fig.11. Active and reactive power delivery: (a) PCC voltage and inverter current; (b) two phases of grid currents; and (c) grid neutral current ($I_{g,n}$) and inverter neutral current ($I_{o,n}$).

C. Active Power Delivery and Unbalance Compensation

The load considered in the system imposes unbalance component to the grid's current. Therefore, the CPT, proposed in the paper, is used to extract the unbalance current/power component of

the load. In this study, the aim is to compensate the unbalance current component caused by the single- and intra phase loads ($i_{ref} = i_{active} + i_u$). Therefore, the inverter current is sinusoidal but unbalanced whereas the grid currents are balanced but non sinusoidal and out of phase with the voltages as shown in Fig. 12(a) and (b) respectively. In this case, the inverter current is responsible for supplying unbalance current component of the single phase loads through its fourth-leg as it is illustrated in Fig. 12(c).

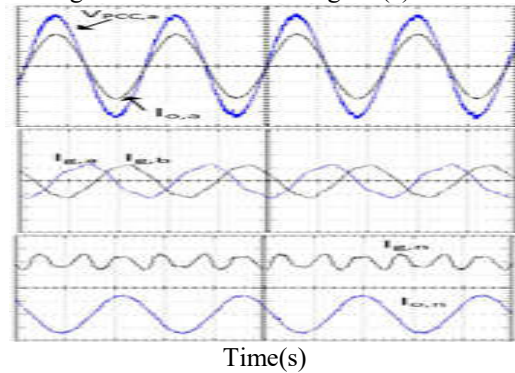


Fig.12. Active power delivery and unbalance compensation: (a) PCC voltage and inverter currents; (b) two phases of grid current; and (c) grid neutral current ($I_{g,n}$) and inverter neutral current ($I_{o,n}$).

Note that the harmonic current component of the single- and three-phase loads is still supplied by the grid. D. Active Power Delivery and Harmonics Compensation At this case study, the inverter is providing harmonics compensation by injecting the void currents ($i_{ref} = i_{active} + i_v$). From Fig. 13(a) and (b), the inverter current is nonlinear whereas the grid current is sinusoidal but unbalanced and not in phase with the voltages. It can be observed that the grid in this case is not supplying the single-phase void current components through its neutral wire rather it is supplied by the inverter through its fourth-leg as illustrated in Fig. 13(c).

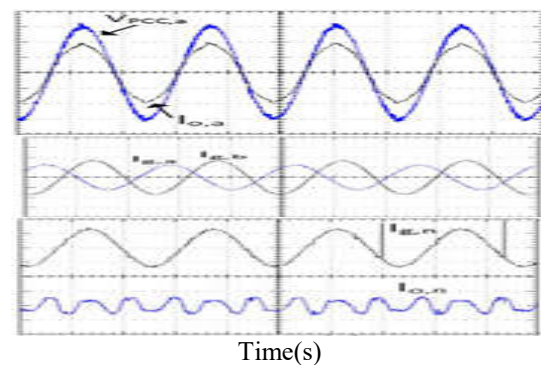


Fig.13. Active power delivery and void compensation: (a) PCC voltage and inverter currents; (b) two phases of grid current; and (c) grid neutral current ($I_{g,n}$) and inverter neutral current ($I_{o,n}$).

The neutral wire of the grid carries only the unbalance current component related to the single-phase loads. E. Active Power Delivery and Non active Compensation in Fig. 14, the inverter is set to compensate non active balanced but non sinusoidal and out of phase with the voltages as shown in Fig. 12(a) and (b) respectively. In this case, the inverter current is responsible for supplying unbalance current component of the single phase loads through its fourth-leg as it is illustrated in Fig. 12(c). Note that the harmonic current component of the single- and three-phase loads is still supplied by the grid. D. Active Power Delivery and Harmonics Compensation At this case study, the inverter is providing harmonics compensation by injecting the void currents ($i_{ref} = i_{active} + i_v$). From Fig. 13(a) and (b), the inverter current is nonlinear whereas the grid current is sinusoidal but unbalanced and not in phase with the voltages.

It can be observed that the grid in this case is not supplying the single-phase void current components through its neutral wire rather it is supplied by the inverter through its fourth-leg as illustrated in Fig. 13(c). The neutral wire of the grid carries only the unbalance current component related to the single-phase loads. E. Active Power Delivery and Non active Compensation In Fig. 14, the inverter is set to compensate non active current component of the load current including all disturbances, i.e., load reactive power, nonlinearities, and unbalances ($i_{ref} = i_{active} + i_{na}$). Fig. 14(a) shows that the inverter current contains non active current component, whereas Fig. 14(b) shows the grid is absorbing the remaining active current which is not consumed by the load. Note that the active current, exported to the grid is proportional to the instantaneous PCC voltages. As shown in Fig. 14(c), the grid supplies zero current through its neutral and the inverter is supplying the return current of single phase loads through its fourth-leg.

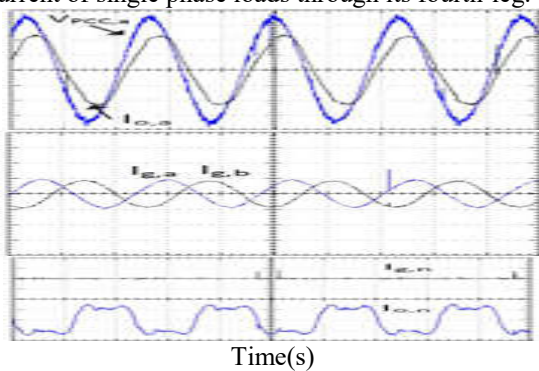


Fig.14. Active power delivery and non-active compensation: (a) PCC voltage and inverter currents; (b) two phases of grid current; and (c) grid neutral current ($I_{g,n}$) and inverter neutral current ($I_{o,n}$).

F. Multifunctional and Active Filter Modes

In this section, two different tests are performed to validate the overall performance of the machine side and the grid side controllers during different wind speed conditions. In Fig. 15, a test is done to validate the controller when it switches from active power delivery only to active and non active compensation at maximum wind power. From Fig. 15, at $t=7$ s, the inverter started providing active power as well as non active compensation. The dc-link voltage starts to oscillate but kept at its desired value.

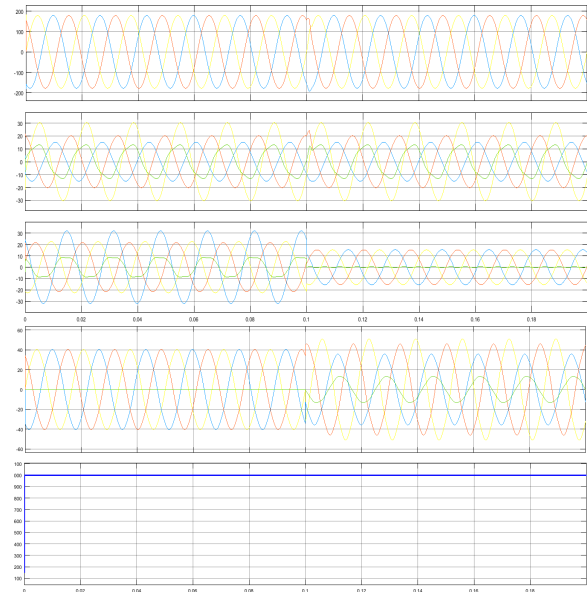
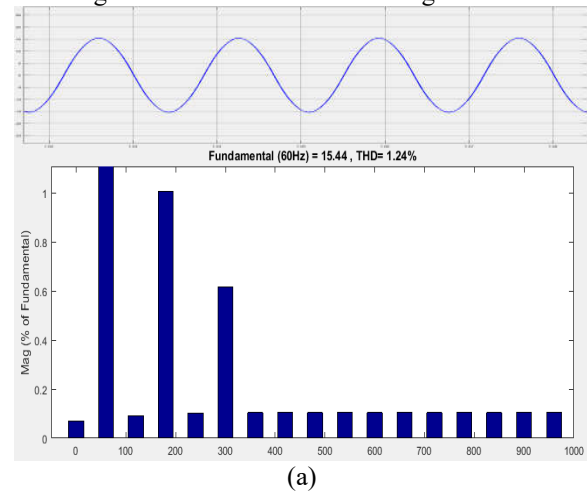
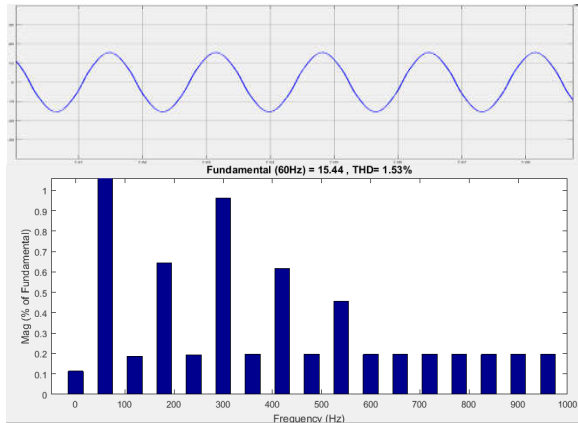


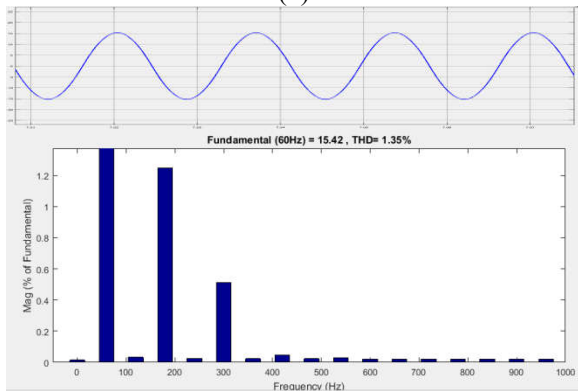
Fig.15. Active power delivery and non-active compensation at $t=7$ s.

The grid current becomes sinusoidal and balanced. The inverter current, on the other hand, becomes unbalanced and nonlinear. The neutral current is produced by the fourth leg of the inverter resulting in zero neutral current at the grid side.





(b)



(c)

Fig.16. Spectrum and THD of grid current without power quality improvement: (a) phase-a; (b) phase-b; and (c) phase-c.

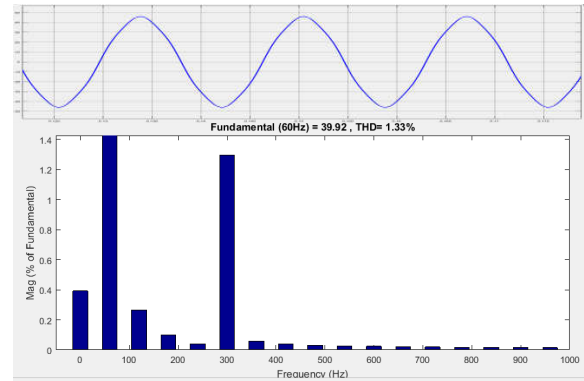
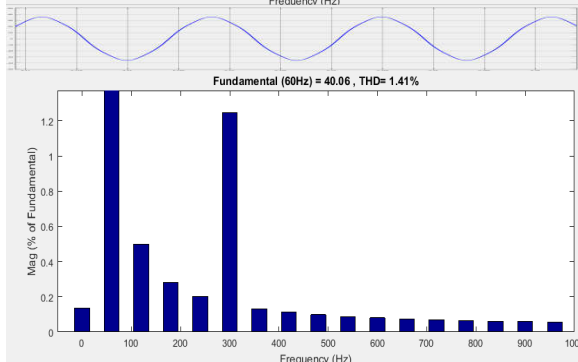
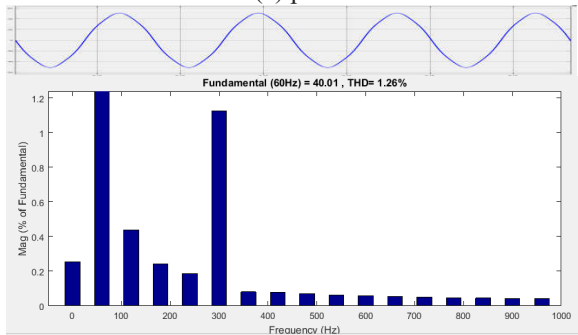


Fig. 17 Spectrum and THD of grid current with non active compensation: (a) phase-a; (b) phase-b; and (c) phase-c.

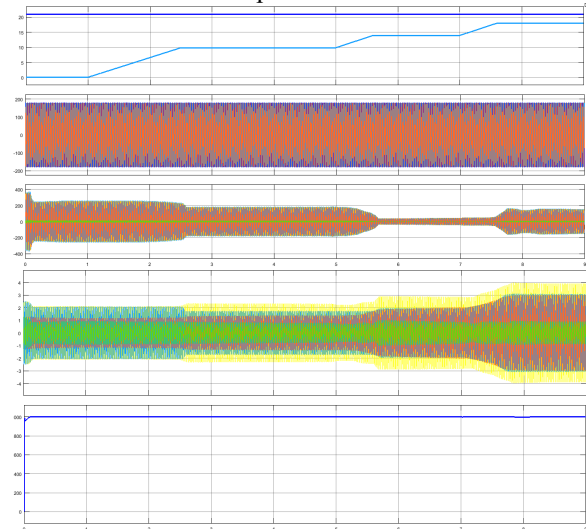


Fig.18 Active power delivery and non-active compensation under different wind speeds

The harmonic spectrum of the grid current and total harmonic distortion (THD) with no compensation is shown Fig. 16. Since there are single- and three-phase loads as well as intra phase loads in the system, the THD is different for each phase. The current of phase-a and phase-c contain THD of 5.84% and 5.35%, respectively.

In Fig. 17, the grid current spectrum is demonstrated after the inverter is set to compensate the load non active current components. The THD of phases-a and phase-c were reduced from 5.84% and 5.35% to about 2.46% and 2.68%, respectively. Phase-b initially had much less harmonics because it does not have nonlinear single-phase load as the other phases. The amplitude of the grid current is reduced as the inverter is also supplying the unbalance components.

In Fig. 18, a comprehensive test is performed under different wind speeds. At no wind available or zero rotor speed, the grid side inverter is operating as active filter. Therefore, the controller is

intended to keep the dc voltage at constant value (1000 V) and provide non active compensation to improve the power quality of the grid current. During this condition, the grid supplies the active power for the load.

6. CONCLUSION

The proposed SVPWM based control scheme for the grid connected Wind energy generation system for power quality improvement is simulated using MATLAB/SIMULINK. The control scheme has a capability to cancel out the harmonic parts of the load current. It maintains the source voltage and current in-phase and supports the reactive power demand for the wind generator and load at PCC in the grid system. The results corroborated our power quality enhancement control and allowed to exclude passive filters, contributing to a more compact, flexible, and reliable electronic implementation of a smart-grid based control.

REFERENCES

- [1] "Global wind report annual market update 2013," 2013.[Online]. Available: <http://www.gwec.net>
- [2] S. Li, T. A. Haskew, R. P. Swatloski, and W. Gathings, "Optimal and direct-current vector control of direct-driven PMSG wind turbines,"IEEE Trans. Power Electron., vol. 27, no. 5, pp. 2325–2337, May 2012.
- [3] N. Angela, M. Liserre, R. A. Mastromauro, and A. D. Aquila, "A survey of control issues in PMSG-based,"IEEE Trans. Ind. Informat., vol. 9, no. 3, pp. 1211–1221, Aug. 2013.
- [4] J.Lagorse, M.G.Simões, and A. Miraoui, "A multiagent fuzzy-logicbased energy management of hybrid systems,"IEEE Trans. Ind. Appl., vol. 45, no. 6, pp. 2123–2129, Nov./Dec. 2009.
- [5] X. Tan, Q. Li, and H. Wang, "Advances and trends of energy storage technology in microgrid," Int. J. Elect. Power Energy Syst., vol. 44, pp. 179–191, Jan. 2013.
- [6] P. F. Ribeiro, B. K. Johnson, M. L. Crow, A. Arsoy, and Y. Liu, "Energy storage systems for advanced power applications,"Proc. IEEE, vol. 89, no. 12, pp. 1744–1756, Dec. 2001.
- [7] M. G. Simoes, B. K. Bose, and R. J. Spiegel, "Fuzzy logic based intelligent control of a variable speed cage machine wind generation system,"IEEE Trans. Power Electron., vol. 12, no. 1, pp. 87–95, Jan. 1997.
- [8] A. Chauhan and R. P. Saini, "A review on integrated renewable energy system based power generation for stand-alone applications: Configurations, storage options, sizing methodologies and control,"Renew. Sustain. Energy Rev., vol. 38, pp. 99–120, Oct. 2014.

[9] C. N. Bhende, S. Mishra, and S. G. Malla, "Permanent magnet synchronous generator-based standalone wind energy supply system,"IEEE Trans. Sustain. Energy, vol. 2, no. 4, pp. 361–373, Oct. 2011.

[10] H. Akagi, E. H. Watanabe, and M. Aredes, "Instantaneous power theory and applications to power conditioning,"IEEE Industrial Electron. Magazine, vol. 1, no. 3, p. 46, Fall 2007.



A SHRAVAN KUMAR

He received B.tech degree in 2016 Electrical and Electronics Engineering from Malla Reddy Engineering College Maisammaguda, Hyderabad and M.tech degree in Electrical and Electronics Engineering Specialization in Electrical Power Systems from Vignana Bharathi Institute of Technology, Hyderabad. The area of interest is Electrical Power Systems.

Chintushraavan280@gmail.com



K VAMSEE KRISHNA

He received B.tech degree in Electrical Engineering from Kakatiya University, Warangal and M.tech degree in Electrical Engineering from OU University Hyderabad. He is currently working in Associate Professor in Vignana Bharathi Institute of Technology, Hyderabad.

kvkbit@gmail.com